Modeling of the Enthalpy Transfer Using Electric Circuit Equivalents: Theory and Application to Transients of Multi-Carrier Energy Systems

Tian Lan and Kai Strunz

***Abstract*—Analogies between electric, hydraulic, and thermal quantities do exist for developing various circuit models that involve quantities such as currents and voltages, flows and pressures, and heat transfers and temperatures. With the increasing interest in multi-carrier energy systems, it would be beneficial to extend the scope of analogies to the enthalpy transfer by advection. The presentation of the concept and the realization of this analogy extension are the purpose of this paper. It is shown how the enthalpy transfer is formulated using circuit equivalents and how they can be used in the modeling of components such as junctions and pipes of multi-carrier energy systems. The theoretical considerations are complemented by validation through comparison with software models and physical experiment. The value of implementing the enthalpy transfer using circuit equivalents is illustrated by the modeling of a combined heat and power multi-carrier energy system implemented in a nodal-analysis-based network simulator of the EMTP type.**

***Index Terms*—Enthalpy transfer, advection, circuit equivalent, multi-carrier energy system, multi-physics component, junction, pipe, combined heat and power.**

NOMENCLATURE

Variables and Operators

A	Area, m^2.
C_{th}	Thermal capacitance, $\mathrm{J}\cdot\mathrm{K}^{-1}$.
c_{p}	Specific heat capacity, $\mathrm{J}\cdot\mathrm{kg}^{-1}\cdot\mathrm{K}^{-1}$.
D	Insulation diameter, m.
d_{i}	Inner pipe diameter, m.
d_{o}	Outer pipe diameter, m.
$\dot{H}$	Enthalpy transfer rate, $\mathrm{J}\cdot\mathrm{s}^{-1}$.
h	Specific enthalpy, $\mathrm{J}\cdot\mathrm{kg}^{-1}$.
$\overline{h}$	Molar enthalpy, $\mathrm{J}\cdot\mathrm{mol}^{-1}$.
h_{f}^{0}	Enthalpy of formation, $\mathrm{J}\cdot\mathrm{kg}^{-1}$.
i	Counter for pipe segment.
K	Pressure loss coefficient, $\mathrm{m}^{-1}\cdot\mathrm{kg}^{-1}$ or $\mathrm{m}^{-1}\cdot\mathrm{kg}\cdot\mathrm{mol}^{-2}$.
k_{cond}	Thermal conductivity, $\mathrm{W}\cdot\mathrm{m}^{-1}\cdot\mathrm{K}^{-1}$.
k_{conv}	Convective heat transfer coefficient, $\mathrm{W}\cdot\mathrm{m}^{-2}\cdot\mathrm{K}^{-1}$.
$k_{\mathrm{conv\text{-}rad}}$	Convective-radiative heat transfer coefficient, $\mathrm{W}\cdot\mathrm{m}^{-2}\cdot\mathrm{K}^{-1}$
M	Number of heat exchanger segments.
m	Mass, kg.
$\dot{m}$	Mass flow rate, $\mathrm{kg}\cdot\mathrm{s}^{-1}$.
N	Number of pipe segments.
$\dot{n}$	Molar flow rate, $\mathrm{mol}\cdot\mathrm{s}^{-1}$.
p	Pressure, Pa.
Δp	Pressure drop of the flow in the pipe, Pa.
$\dot{Q}$	Heat transfer rate, $\mathrm{J}\cdot\mathrm{s}^{-1}$.
R_{th}	Thermal resistance, $\mathrm{K}\cdot\mathrm{W}^{-1}$.
R_{fl}	Flow resistance, $\mathrm{Pa}\cdot\mathrm{s}\cdot\mathrm{kg}^{-1}$ or $\mathrm{Pa}\cdot\mathrm{s}\cdot\mathrm{mol}^{-1}$.
r	Radius, m.
T	Thermodynamic temperature, K.
t	Time, s.
Δx	Length of pipe segment, m.
z	Depth of water in tank, m.
∂	Partial difference operator.
ρ	Density, $\mathrm{kg}\cdot\mathrm{m}^{-3}$.
λ	Darcy friction factor, dimensionless.
δ	Heat exchanger wall plate thickness, m.

Subscripts

a	Ambient.
c	Combined conductive, convective, and radiative.
cond	Conductive.
conv	Convective.
dw	Domestic water.
exh	Exhaust stream.
f	Formation.
fl	Flow.
hex	Heat exchanger.
i	In.
ini	Initial.
ins	Insulation.
o	Out.
p	Pipe
rad	Radiation.
ref	Reference.
src	Source.
stor	Storage.
th	Thermal.
w	Wall.

Manuscript received January 19, 2018; revised May 21, 2018; accepted July 19, 2018. Date of publication January 7, 2019; date of current version November 21, 2019. *(Corresponding author: Kai Strunz.)*

The authors are with the Sustainable Electric Networks and Sources of Energy, Technische Universität Berlin, 10587 Berlin, Germany.

Color versions of one or more of the figures in this paper are available online at http://ieeexplore.ieee.org.

Digital Object Identifier 10.1109/TEC.2019.2891345

This work is licensed under a Creative Commons Attribution 4.0 License. For more information, see https://creativecommons.org/licenses/by/4.0/

TABLE I
ANALOGIES BETWEEN ELECTRICAL AND THERMAL QUANTITIES

Quantity	Electric	Thermal
Potential	Electrostatic potential ϕ (V)	Thermodynamic temperature T (K)
Flow	Current I (A)	Heat transfer $\dot{Q}$ $(\mathrm{J}\cdot\mathrm{s}^{-1})$
Resistance	Electric resistance R (Ω)	Thermal resistance R_{th} $(\mathrm{K}\cdot\mathrm{W}^{-1})$
Capacitance	Electric capacitance C (F)	Thermal capacitance C_{th} $(\mathrm{J}\cdot\mathrm{K}^{-1})$

I. INTRODUCTION

ANALOGIES between electric and thermal circuits have been effective and illustrative [1]–[5]. By exploiting the analogies, it is possible to apply the knowledge of one field to another. Table I presents some already evident analogies between electric and thermal quantities. It is shown that both thermodynamic temperature and electrostatic potential represent a potential. Heat transfer by conduction is in analogy to the current. The current is caused by a voltage difference, the process of which is similar to that of heat transfer by conduction as driven by a temperature difference. The analogy of Table I may also be applied to other forms of heat transfer caused by temperature difference.

According to the U.S. Department of Energy (DOE), Combined Heat and Power (CHP) systems are under rapid development and have promising potential [6]. In order to effectively utilize CHP in practical power systems, it is important to study the transfer of multiple energy carriers within the networks connected to the CHP [7]–[12]. In CHP systems, an important means of transferring energy is by advection. The latter is an energy transfer mechanism due to a bulk motion of fluid. Thus, advection is different from the heat transfer, which by definition is caused by a temperature difference. The energy transfer by advection has not yet been included in the scope of analogies between electric and thermal quantities of Table I. Therefore, to support the understanding of this means of energy transfer, an extension of the analogies to also cover the enthalpy transfer by advection appears to be valuable. Moreover, with such an extension, it would be possible to analyze that enthalpy transfer using circuit equivalents. This will facilitate their modeling in circuit-oriented simulators, such as the EMTP (Electromagnetic Transients Program) or variations [13]–[16].

Compared with the electric power flow that can be obtained from current and voltage, the enthalpy transfer by advection is determined by the mass flow rate and the temperature of the fluid. It gives the energy transported by the moving fluid in the pipe. Although the analogies between current and heat transfer as well as electrostatic potential and temperature do exist, this enthalpy transfer by advection is not driven by a temperature difference, instead it is driven by a difference in pressure. A formulation of an analogy to Ohm's law is therefore not possible. This important variation brings challenges to the modeling of the enthalpy transfer using circuit equivalents.

In Section II, the modeling of the enthalpy transfer using circuit equivalents is proposed. Next, based on the formulation, the equivalent circuits for modeling multi-physics components including junction and pipe as fundamental elements in heat networks are described in Sections III and IV, respectively. The validation of the developed model for steady state and transient operation is presented in Section V. A test case demonstrating a district heating application realized using electric circuits is given in Section VI. Conclusions are drawn in Section VII.

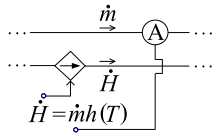

Fig. 1. Electrical analogue of enthalpy transfer by advection.

II. CONCEPT

The analogies presented in Table I have been used in various applications involving multiple energy carriers [17]–[21]. In [17], the thermodynamic characteristics inside a Proton Exchange Membrane Fuel Cell (PEMFC) were described using electric circuits based on electrical analogues of thermal quantities. In [18]–[21], the thermal-electric analogy was applied to transformer thermal modeling in a way that temperature responses of the transformers can be calculated using circuit equivalents. Despite being useful for certain types of studies, the currently available analogies between multi-physics quantities do not have the enthalpy transfer in general involved.

Of key interest in this paper is the enthalpy transfer by advection, which is found in district heating networks and is defined as follows:

$$\dot{H} = \dot{m} \cdot h(T) \tag{1}$$

where $\dot{m}$ is the mass flow rate of a fluid, $\dot{H}$ is the enthalpy transfer rate affiliated with $\dot{m}$, and h is the specific enthalpy of the fluid at temperature T. The specific enthalpy h can be obtained by adding the specific enthalpy change Δh between the standard state T_0 and the current state T to the enthalpy of formation h_{f}^0 as given in the following [5]:

$$\begin{aligned} h(T) &= h_{\mathrm{f}}^0 + \Delta h(T) \\ &= h_{\mathrm{f}}^0 + c_{\mathrm{p}}(T - T_0) \end{aligned} \tag{2}$$

where c_{p} is the specific heat capacity of the fluid.

As defined in (1), the considered enthalpy transfer rate $\dot{H}$ is determined by the mass flow rate $\dot{m}$ and temperature T of a fluid. The flow of a fluid can be driven by pressure difference. A fluid may also flow from a lower temperature level to a higher temperature level, indicating that the enthalpy can migrate along with the flowing fluid from one control volume to another regardless of the temperature difference. Based on the above observations, the enthalpy transfer by advection can be modeled by a controlled current source, whose controlling signal is the flow rate of the fluid. The proposed circuit implementation is shown in Fig. 1. According to the analogy given in Table I, the mass flow rate of a fluid $\dot{m}$ can be implemented as a current flowing through a circuit as depicted on the upper line of Fig. 1. The enthalpy transfer rate $\dot{H}$ affiliated with the flowing fluid $\dot{m}$ is

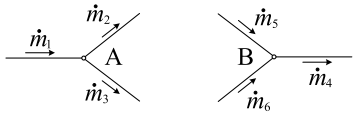

Fig. 2. Junction schematic showing mass flows.

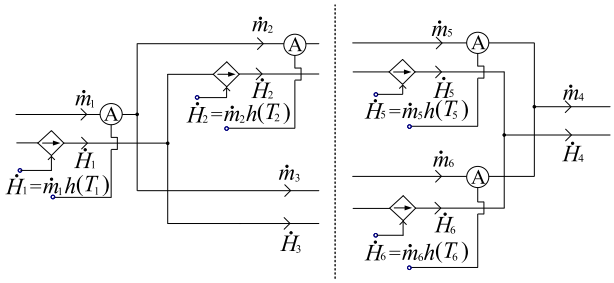

Fig. 3. Implementation of model for junction as equivalent circuit.

implemented as a current-controlled current source. The flow rate $\dot{m}$ is measured in the upper circuit and used for calculating the controlling signal of the current-controlled current source as depicted in the lower-side circuit of Fig. 1.

To facilitate the modeling of the components in the following sections, selected assumptions have been introduced regarding geometry, fluid characteristics, and heat transfer. The list of assumptions is given in Appendix A.

III. Modeling of Junction

The junctions are comparable to nodes within the electrical network. According to assumption 1 of Appendix A, the sum of all flows entering a node equals the sum of all flows leaving this node [22]. It reflects the law of conservation of mass at each node. In circuit analysis, it is known as the Kirchhoff's current law. Moreover, there is no energy loss to the environment, hence enthalpy is conserved, and there is no overall entropy change.

A. Mathematical Description

In Fig. 2, two junctions as used in the heat network are depicted. Regarding the node A on the left side of Fig. 2, the following expression can be established reflecting the conservation of mass [22]:

$$\dot{m}_1 - \dot{m}_2 - \dot{m}_3 = 0. \tag{3}$$

In (3), $\dot{m}_i$ is given a positive sign if the convention in Fig. 3 shows it flowing to the node; otherwise it comes with a negative sign.

As the junctions are assumed as nodes that cannot store energy, the enthalpy transfer balance equation of node A in Fig. 2 is given by:

$$\dot{H}_1 - \dot{H}_2 - \dot{H}_3 = 0, \tag{4}$$

where

$$\dot{H}_1 = \dot{m}_1 h(T_1), \tag{5}$$

$$\dot{H}_2 = \dot{m}_2 h(T_2), \tag{6}$$

$$\dot{H}_3 = \dot{m}_3 h(T_3). \tag{7}$$

Similarly, for the node B on the right side of Fig. 2, the mass flow and enthalpy transfer balances can be, respectively, given by:

$$\dot{m}_4 - \dot{m}_5 - \dot{m}_6 = 0. \tag{8}$$

$$\dot{H}_4 - \dot{H}_5 - \dot{H}_6 = 0. \tag{9}$$

With an implementation of the pipe as to be introduced in the following Section IV, the temperatures of the fluids flowing out of the nodes, such as T_2, T_3, and T_4, can be measured.

B. Formulation for Circuit Equivalents

Fig. 3 shows the circuit implementation of the two junctions of Fig. 2. On the left side of Fig. 3, the representation of node A is depicted. It is implemented based on the mass flow balance and enthalpy transfer balance given in (3) and (4), respectively. In the electric circuit analogy, (3) can be implemented as a node. Three currents indicating three flows meet at a common node to realize the mass flow balance. The affiliated enthalpy transfers discussed in Section II are modeled as current-controlled current sources as shown in the figure. The controlling signal $\dot{m}$ is taken by obtaining the current signal from the mass flow circuit. As $\dot{H}_1$ and $\dot{H}_2$ are modeled as current sources, $\dot{H}_3$ is then readily given due to (4).

Regarding node B in Fig. 2, the implementation is similar as for node A. Balances given in (8) and (9) can be implemented as shown on the right side of Fig. 3. Enthalpy transfers $\dot{H}_5$ and $\dot{H}_6$, modeled as current-controlled current sources, meet at a node and in sum give the output enthalpy transfer $\dot{H}_4$.

IV. Modeling of Pipe

Pipes in a heating network are used for advecting enthalpy. As opposed to nodes, pipes are of spatial dimension. Pipes possess a volume and can therefore store energy within their contained fluid, allowing for transient behavior of the temperature within district heating networks. According to assumptions 2 and 3 of Appendix A, conservation of mass inside the control volume is assumed, and changes of potential or kinetic energies are disregarded. Also applicable are the assumptions 4, 5, and 6 of Appendix A.

A. Mathematical Description

The temperature of the fluid in a pipe is a function of time and location of the moving fluid. The considered pipe is of cylindrical shape. Fig. 4 shows the considered differential control volume inside the pipe and associated energy interactions in accordance with assumptions 3 and 4. The control volume represents a pipe segment of length $\mathrm{d}x$. The bulk motion of the fluid is along the indicated x-axis. The energy conservation is as follows:

$$\frac{\partial H}{\partial t \partial x}\mathrm{d}x = -\frac{\partial \dot{H}}{\partial x}\mathrm{d}x - \frac{\partial \dot{Q}_\mathrm{c}}{\partial x}\mathrm{d}x. \tag{10}$$

The left-hand side of the equation gives the differential change of enthalpy inside the control volume. The first term on the right-hand side gives the negative of the differential enthalpy advected in axial x-direction out of the control volume. Further

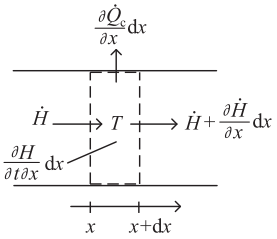

Fig. 4. Differential control volume of infinitesimal length $\mathrm{d}x$ in pipe.

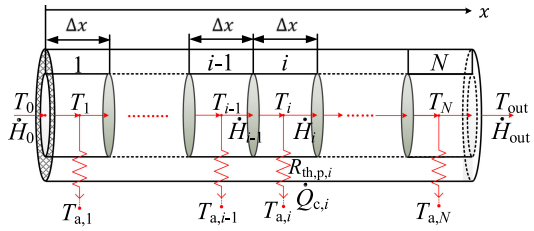

Fig. 5. Segmentation of pipe into control volumes of length Δx.

subtracted is the heat transfer rate normal to the x-direction, also by convention positive when leaving the control volume. This heat transfer is a combined process of convection at the inner surface of the pipe, conduction through the pipe wall and potential insulation layer, while at the outer surface convection and radiation are to be considered in general.

Omitting $\mathrm{d}x$ in (10) yields a formulation in per unit length:

$$\frac{\partial H}{\partial t \partial x} = -\frac{\partial \dot{H}}{\partial x} - \frac{\partial \dot{Q}_{\mathrm{c}}}{\partial x}. \tag{11}$$

This expression can be extended to give an advection equation for temperature T inside the pipe:

$$\rho A c_{\mathrm{p}} \frac{\partial T}{\partial t} = -\dot{m} c_{\mathrm{p}} \frac{\partial T}{\partial x} - G'_{\mathrm{th,p}}(T - T_{\mathrm{a}}), \tag{12}$$

with

$$G'_{\mathrm{th,p}} = \frac{\partial G_{\mathrm{th,p}}}{\partial x}, \tag{13}$$

where T giving the temperature of the fluid in the control volume is a function of space and time $T(x,t)$; T_{a} is the ambient temperature of the pipe; $\dot{m}$ as the mass flow rate of the incompressible fluid acts as a time-variant quantity $\dot{m}(t)$, which is by convention positive when it flows toward increasing values of x. Furthermore, ρ is the density of the fluid, c_{p} is the specific heat capacity of the fluid, and A is the inner cross section area of the pipe segment. Density ρ and specific heat capacity c_{p} are considered to be constant according to assumption 5 of Appendix A [5], [22]. In accordance with assumption 6, the flow is considered in the fully developed region along the pipe. The last term on the right side of (12) is defined as positive when the temperature T inside exceeds the ambient temperature T_{a}, $T > T_{\mathrm{a}}$. Quantity $G'_{\mathrm{th,p}}$ is the combined convective, conductive, and radiative thermal conductance of the pipe wall and potential insulation per unit length.

Equation (12) is a time-dependent partial differential equation (PDE). In order to solve (12), numerical computation is applied. Assuming a spatial discretization into the segments $\{1, 2, \ldots, N\}$ as shown in Fig. 5, a pipe can be split into N segments along the flow path, and Δx is the length of each segment. Thereafter, an upwind difference approximation is applied to the spatial derivative of T [23]:

$$\left(\frac{\partial T}{\partial x}\right)_i = \frac{T_i - T_{i-1}}{\Delta x}; \quad T_i(t) = T(x_i, t),\ i = 1, 2, \ldots, N. \tag{14}$$

Combining (14) with (12) and multiplication by Δx leads to a system of ordinary differential equations in the variable t given by:

$$\rho A c_{\mathrm{p}} \Delta x \frac{\mathrm{d}T_i}{\mathrm{d}t} = -\dot{m} c_{\mathrm{p}} (T_i - T_{i-1}) - G_{\mathrm{th,p},i}(T_i - T_{\mathrm{a},i});\ i = 1, 2, \ldots, N \tag{15}$$

The transition from (10) to (15) also marks the transition from a differential control volume of length $\mathrm{d}x$ to a control volume of finite length Δx. In Fig. 5, the segmentation into control volumes is illustrated. For pipe segment i, (15) can be rewritten as:

$$C_{\mathrm{th,p},i} \frac{\mathrm{d}T_i}{\mathrm{d}t} = \dot{H}_{i-1} - \dot{H}_i - \dot{Q}_{\mathrm{c},i}, \tag{16}$$

with

$$\dot{H}_i = \dot{m} h(T_i), \tag{17}$$

$$\dot{H}_{i-1} = \dot{m} h(T_{i-1}), \tag{18}$$

$$\dot{Q}_{\mathrm{c},i} = G_{\mathrm{th,p},i}(T_i - T_{\mathrm{a},i}), \tag{19}$$

where $\dot{H}_{i-1}$ and $\dot{H}_i$, as shown in Fig. 5, are the enthalpy transfers associated with the bulk fluid flows at the inlet and outlet of the pipe segment i, respectively, $\dot{Q}_{\mathrm{c},i}$ is the heat transfer from the fluid to the ambient, and specific enthalpy h can be obtained according to (2). Capacitance $C_{\mathrm{th,p},i}$ is the thermal capacitance of the mass of the fluid in the pipe segment, and $G_{\mathrm{th,p},i}$ is the overall thermal conductance encountered by $\dot{Q}_{\mathrm{c},i}$ of the pipe segment. The capacitance is found by comparison of (15) and (16):

$$C_{\mathrm{th,p},i} = \rho A c_{\mathrm{p}} \Delta x. \tag{20}$$

As the heat transfer from the fluid close to the inner surface of the pipe toward the ambient covers several sequential processes, all driven by temperature drops that add up to the total temperature drop, it is convenient to express the conductance by a resistance:

$$R_{\mathrm{th,p},i} = \frac{1}{G_{\mathrm{th,p},i}}. \tag{21}$$

Fig. 6 shows the cross section of a pipe segment. Heat is transferred by the following processes: convection inside the fluid close to the surface toward the surface of the pipe wall; conduction across the pipe wall and, if available, the insulation layer; as well as convection in the fluid close to the outer surface normal to the surface plus potentially significant radiation if the

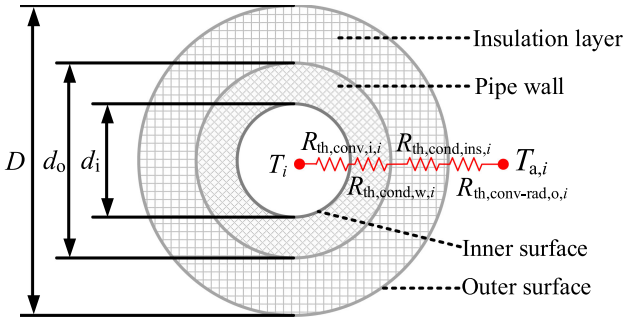

Fig. 6. Cross section of pipe segment i.

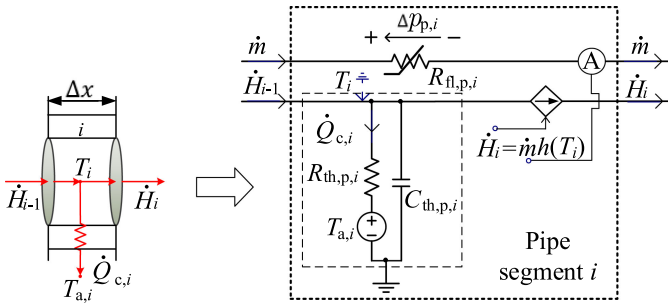

Fig. 7. Implementation of model for pipe segment as equivalent circuit.

surface is exposed to a gas. The overall thermal resistance of this combined process of convection, conduction, and radiation becomes:

$$R_{\mathrm{th,p},i} = R_{\mathrm{th,conv,i},i} + R_{\mathrm{th,cond,w},i} + R_{\mathrm{th,cond,ins},i} + R_{\mathrm{th,conv\text{-}rad,o},i}, \quad (22)$$

where $R_{\mathrm{th,conv,i},i}$ is the inner side convection thermal resistance of the segment, $R_{\mathrm{th,cond,w},i}$ and $R_{\mathrm{th,cond,ins},i}$ are the pipe wall and insulation layer conduction thermal resistances of the segment, respectively, and $R_{\mathrm{th,conv\text{-}rad,o},i}$ is the outer side convection and radiation thermal resistance of the segment. They can be expressed by:

$$R_{\mathrm{th,conv,i},i} = \frac{1}{k_{\mathrm{conv,i},i}\pi d_{\mathrm{i}}\Delta x}, \quad (23)$$

$$R_{\mathrm{th,cond,w},i} = \frac{\ln\left(\frac{d_{\mathrm{o}}}{d_i}\right)}{k_{\mathrm{cond,w},i}2\pi\Delta x}, \quad (24)$$

$$R_{\mathrm{th,cond,ins},i} = \frac{\ln\left(\frac{D}{d_{\mathrm{o}}}\right)}{k_{\mathrm{cond,ins},i}2\pi\Delta x}, \quad (25)$$

$$R_{\mathrm{th,conv\text{-}rad,o},i} = \frac{1}{k_{\mathrm{conv\text{-}rad,o},i}\pi D\Delta x}. \quad (26)$$

where $k_{\mathrm{conv,i},i}$ denotes a convection heat transfer coefficient; $k_{\mathrm{cond,w},i}$ and $k_{\mathrm{cond,ins},i}$ give thermal conductivities; $k_{\mathrm{conv\text{-}rad,o},i}$ is the combined convection and radiation heat transfer coefficient [4].

The thermal resistances on the right side of (22) may heavily vary with respect to different applications. For instance, pipes are usually buried underground in district heating applications. In this case, the ambient side thermal resistance due to convection and radiation $R_{\mathrm{th,conv\text{-}rad,o},i}$ can be neglected from (22). In applications where the insulation layer is not needed for the pipe, $R_{\mathrm{th,cond,ins},i}$ can be neglected in (22).

The pressure drop $\Delta p_{\mathrm{p},i}$ in the flow direction in the pipe segment due to wall friction can be calculated by:

$$\Delta p_{\mathrm{p},i} = K_{\mathrm{p}}|\dot{m}|\dot{m}, \quad (27)$$

where K_{p} is the pressure loss coefficient of the pipe segment and can be expressed as [24]:

$$K_{\mathrm{p}} = \frac{8\lambda\Delta x}{d_{\mathrm{i}}^5\pi^2\rho}, \quad (28)$$

where λ is the Darcy friction factor that is dependent on the Reynolds number and flow cross section geometry, and d_{i} is the inner pipe diameter. The applied sign convention of (27), illustrated in Fig. 7, supports the modeling of a flow resistance as follows:

$$R_{\mathrm{fl,p},i} = \frac{\Delta p_{\mathrm{p},i}}{\dot{m}}, \quad (29)$$

where $R_{\mathrm{fl,p},i}$ is variable. By inspection of (27), it is expressed as:

$$R_{\mathrm{fl,p},i} = K_{\mathrm{p}}|\dot{m}|. \quad (30)$$

B. Formulation Using Circuit Equivalents

Based on the established discretized pipe equations, a π-model can be implemented for representing the enthalpy distribution pipe in analogy to the π-circuit model used for modeling lines in electric power networks. In this context, (16) describing the thermal transients in a pipe segment is represented using the lower circuits within the frame of Fig. 7. Enthalpy transfer $\dot{H}_{i-1}$ incoming from the prior pipe segment enters to a parallel combination of a resistive branch, a capacitive branch, and a controlled current source branch with the enthalpy transfer output from the present segment. The resistive branch consists of a resistance $R_{\mathrm{th,p},i}$, which comprises four thermal resistances as given in (22). It is connected to a voltage source giving the ambient temperature $T_{\mathrm{a},i}$. The quantity $\dot{Q}_{\mathrm{c},i}$ in this branch is the heat transfer from inside the pipe normal to the pipe wall to the ambient. The capacitive branch consists of a thermal capacitance $C_{\mathrm{th,p},i}$, impacting the thermal transients of the pipe segment. Based on (16), the outlet enthalpy transfer rate $\dot{H}_i = \dot{m}h(T_i)$ is implemented using a current-controlled current source. Using the electric circuit analogy, the temperature of the water in pipe segment i is obtained by measuring the voltage across the capacitance $C_{\mathrm{th,p},i}$ of Fig. 7.

To model the mass flow of water $\dot{m}$, the pipe is represented using a parallel circuit given in the upper part within the frame of Fig. 7. The flow resistance $R_{\mathrm{fl,p},i}$ is determined by (30). The voltage drop across the flow resistance represents the pressure drop of the water flowing in the pipe segment according to (27).

Connecting all the N pipe segments together in series, a π-model for the pipe can be realized as shown in Fig. 8. Each segment has a length of Δx as in Fig. 5. The values of capacitance $C_{\mathrm{th,p},i}$, of resistances $R_{\mathrm{th,p},i}$ and $R_{\mathrm{fl,p},i}$ are the same for

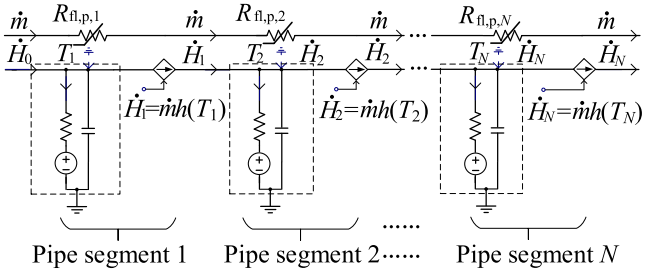

Fig. 8. Implementation of π-model for pipe as equivalent circuit.

TABLE II
MODEL PARAMETERS USED IN VALIDATION

ρ (kg/m^3)	1000	c_p (J/(kg · K))	4190
d_i (m)	0.065	$k_\mathrm{conv,i}$ (W/(m^2 · K))	100
d_o (m)	0.076	$k_\mathrm{cond,w}$ (W/(m · K))	24
D (m)	0.18	$k_\mathrm{cond,ins}$ (W/(m · K))	0.027
T_a (K)	283	λ	0.025

the pipe segments. They can be calculated separately based on (20) to (26), and (30). It is noted that the flow resistances $R_{\mathrm{fl,p},i}$ for each pipe segment may be aggregated for the entire pipe comprising N segments: $R_\mathrm{fl,p} = \sum_{i=1}^{N} R_{\mathrm{fl,p},i}$.

V. VALIDATION

The pipe model is validated for steady state and transients. The validation is carried out with two test cases. The pipe is assumed to be used in a district heating application and buried underground. Therefore, the ambient side thermal resistance due to convection and radiation is neglected. The pipe in district heating applications consists of a carrier pipe with an insulation layer. Parameters used for validating the pipe are given in Table II. The given parameters do not vary in axial direction. The circuit equivalent models were implemented in PSCAD as an EMTP-type program. Equations (20) to (26), and (30) are implemented through Continuous System Model Functions (CSMF) blocks to compute capacitances and resistances. The performance of the circuit-equivalent-based pipe model is first verified by comparing the results to those determined with dedicated software. Furthermore, the performance of the pipe model is validated by comparing the simulation results with measurement data.

A. Comparison with Software Model

The temperature transients affiliated with water flowing in a pipe are studied through a step response. The length of the pipe is set to 100 m. At the beginning at time $t = 0$ s, feeding water temperature T_in and the temperature T_0 of the water initially stored in the pipe are at 363 K. The mass flow of the feeding water is kept at 1 kg/s throughout the simulation. At the time instant $t = 500$ s, there is a temperature drop of 10 K in the feeding water. Different locational discretizations of the pipe are shown to lead to different temperature responses. In Fig. 9, the simulated temperature responses of the

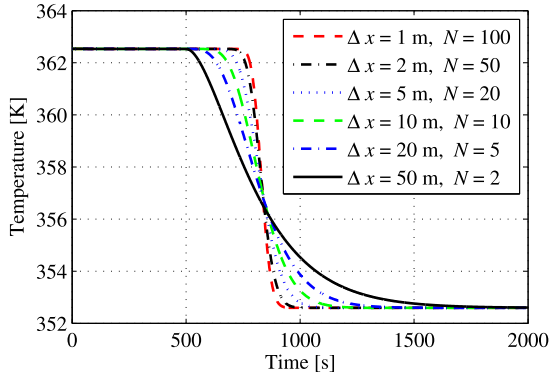

Fig. 9. Pipe model responses to temperature change at different discretizations.

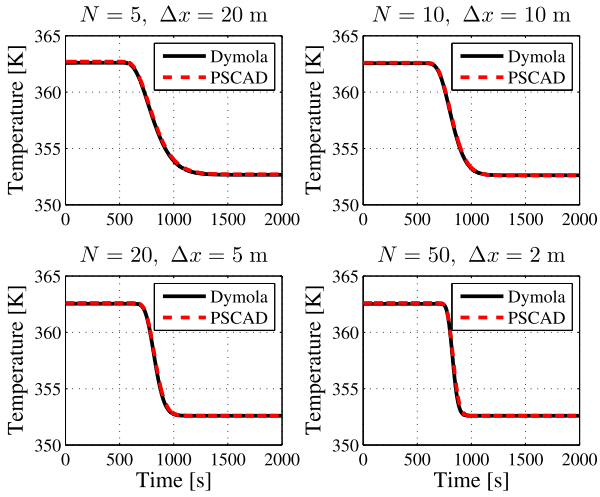

Fig. 10. Pipe model responses to temperature change compared with results given by Dymola.

water at the outlet of the pipe are given. Several observations can be made. At steady state, temperatures at the output are the same for different discretizations. During transients, however, the number of discretization intervals is important in determining the solution. On the one hand, a small number of π-sections may result in a rather inaccurate solution. As an example, for the setting of $\Delta x = 50$ m, $N = 2$, it can be seen that the water temperature at the outlet of the pipe changes almost at the same time as does the temperature step at the inlet. However, this misrepresents the time needed for the water to travel. Too many π-section, on the other hand, would increase the required computational efforts without giving a corresponding gain in accuracy.

The equivalent circuit based pipe model as implemented in PSCAD can be verified by comparing the results with those given by an existing pipe model available in Dymola, a commonly distributed environment for multi-engineering modeling and simulation. The results, depicted in Fig. 10, are in very close agreement. The time step size used for the comparison in Fig. 10 was 1 s for both PSCAD and Dymola. While the dedicated pipe model of Dymola did run faster, it should be noted that dedicated speed optimizations were not applied for the model where the enthalpy transfer is represented in the circuit equivalent. In fact,

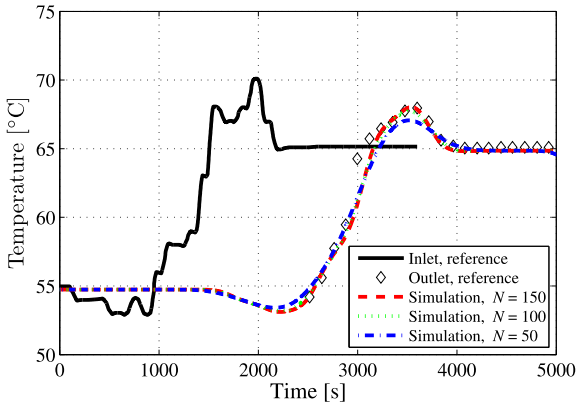

Fig. 11. Pipe model responses to temperature change compared with physical reality.

a main application of the pipe model is to be seen in the context of multi-carrier networks that involve multi-carrier energy systems. The latter can cover AC and DC electric distribution networks [25], [26] together with heat distribution networks.

B. Comparison with Physical Experiment

In this section, the pipe model is validated based on actual data from a physical experiment. In accordance with [27], a pipe of a length of 729 m is used for delivering thermal energy from a heating plant to a heating substation. The parameters of the pipe are given in Table II. The mass flow is 1.45 kg/s. The supply temperature at the heating plant, in the range of 53 °C–70 °C, is depicted with the solid curve as shown in Fig. 11 [27]. The temperature wave propagates away from the heating plant and is measured at the substation. The measurements at the outlet are presented by diamond symbols. Simulations are carried out with three different discretizations, giving 50, 100, and 150 pipe segments, respectively. The results are depicted in Fig. 11. For the simulation runs at $N = 150$ and $N = 100$, the numerical results closely approximate reality. At $N = 50$, due to larger segments, the deviations to the measured data during transients become more pronounced.

VI. Application

In this section, the proposed modeling of the enthalpy transfer is applied in a case study. Thermal power is generated by a Solid Oxide Fuel Cell (SOFC), whose modeling also received attention recently [28]–[30]. It is utilized in a CHP configuration to warm up domestic water. The implementation of the system is shown in Fig. 12. The system is composed of an SOFC-CHP, a heat exchanger, a domestic water supply unit, a water storage unit, and a set of pipes. For any fluid in the model, the mass flow and the enthalpy transfer appear as a pair as shown in Fig. 1. The SOFC-CHP is connected to an electric load indicated by a variable resistance. The exhaust streams out of the SOFC-CHP are used for warming up domestic water in the heat exchanger that is implemented in the block "Heat exchanger power stage". In the domestic water supply unit, cold water is provided. After being warmed up, the water is stored in the block "Water storage"

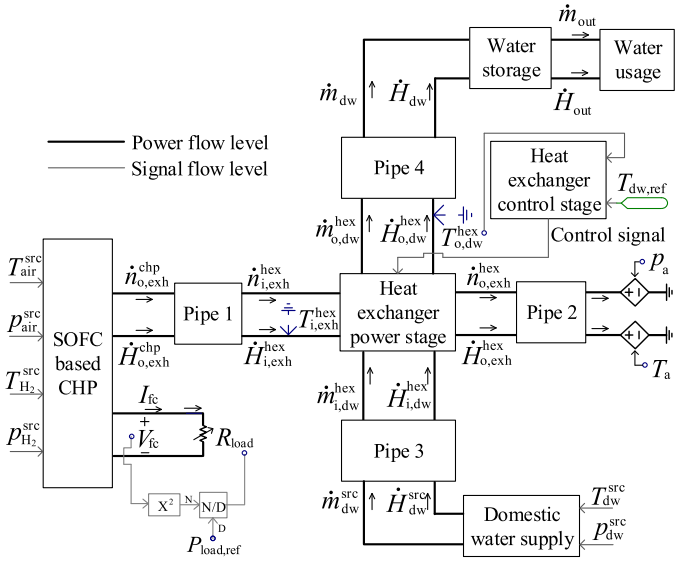

Fig. 12. Implementation of CHP application case in PSCAD.

TABLE III
Model Parameters Used in Application

Model parameters associated with pipe 1 and pipe 2			
d_i (m)	0.086	$k_{\mathrm{conv,i}}$ (W/(m^2 · K))	50
d_o (m)	0.096	$k_{\mathrm{cond,w}}$ (W/(m · K))	24
D (m)	0.12	$k_{\mathrm{cond,ins}}$ (W/(m · K))	0.027
Length (m)	3	$k_{\mathrm{conv\text{-}rad,o}}$ (W/(m^2 · K))	20
Δx (m)	0.2	λ	0.025
N	15	–	–
Model parameters associated with pipe 3 and pipe 4			
d_i (m)	0.015	$k_{\mathrm{conv,i}}$ (W/(m^2 · K))	100
d_o (m)	0.02	$k_{\mathrm{cond,w}}$ (W/(m · K))	24
D (m)	0.04	$k_{\mathrm{cond,ins}}$ (W/(m · K))	0.027
Length (m)	5	$k_{\mathrm{conv\text{-}rad,o}}$ (W/(m^2 · K))	20
Δx (m)	0.2	λ	0.025
N	25	–	–
Model parameters associated with heat exchanger			
A_{exh} (m^2)	1.5	$k_{\mathrm{conv,exh}}$ (W/(m^2 · K))	50
A_w (m^2)	1.5	$k_{\mathrm{cond,w}}$ (W/(m · K))	380
A_{dw} (m^2)	1.5	$k_{\mathrm{conv,dw}}$ (W/(m^2 · K))	100
K_{exh} (kg/(m · mol^2))	0.3	K_{dw} (1/(m · kg))	5598
M	5	δ_w (m)	0.007
Other parameters			
T_a (K)	298	p_a (Pa)	101325
$T^{\mathrm{src}}_{\mathrm{air}}$ (K)	298	$p^{\mathrm{src}}_{\mathrm{air}}$ (Pa)	$1.2p_\mathrm{a}$
$T^{\mathrm{src}}_{\mathrm{H_2}}$ (K)	298	$p^{\mathrm{src}}_{\mathrm{H_2}}$ (Pa)	$10p_\mathrm{a}$
$T^{\mathrm{src}}_{\mathrm{dw}}$ (K)	283	$p^{\mathrm{src}}_{\mathrm{dw}}$ (Pa)	$3p_\mathrm{a}$

for the future usage. Modeling details of these components are given in Appendix B. Parameters used in the application are listed in Table III. The given parameters do not vary in the directions of the mass flows. The pipes of Fig. 12 are exposed to the surrounding air. Therefore, the combined convection and radiation thermal resistance at the outer surface is considered. However, due to the very low conductivity of the insulation layer, the overall thermal resistance is dominated by the conduction thermal resistance of the insulation layer. Regarding the

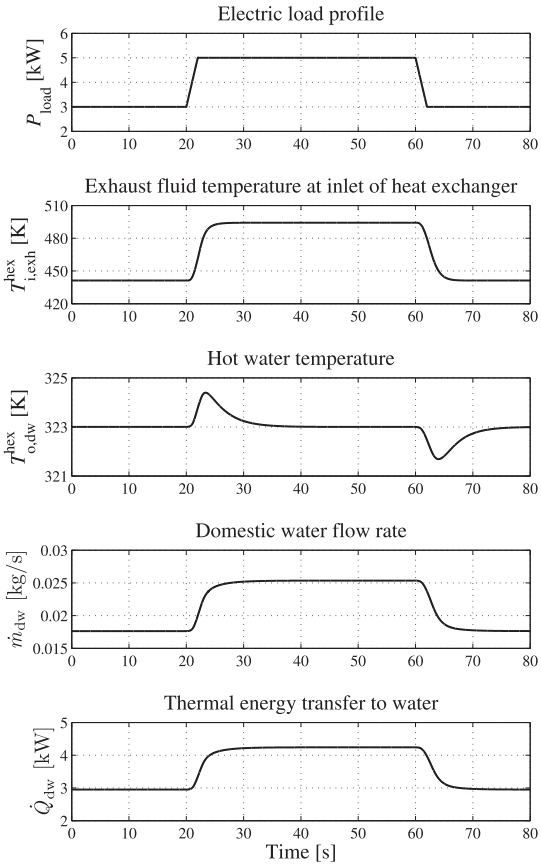

Fig. 13. CHP model responses to electric load change.

heat exchanger, the radiation effect is not considered according to assumption 7 of Appendix A.

The setup in Fig. 12 illustrates how the modeling of the enthalpy transfer is applied to represent and compute the interaction of multi-energy system. It is also shown how the multi-physics components, involving electric, fluid, and thermal quantities, are interfaced with each other using circuitry. For domestic hot water preparation, it is important to control the temperature to a comfortable level. In order to do so, the "Heat exchanger control stage" acts on the "Heat exchanger power stage" to adapt the cold water supply.

A. Thermal Transient of Exhaust Stream

The SOFC-CHP model is a thermally self-sustaining CHP system that is detailed in [28]. In this application, the CHP system comprises a 5-kW SOFC stack, an afterburner, two preheaters, a hydrogen supply system, and an air supply system, with parameters specified in [28]. As depicted in Fig. 12, the SOFC-CHP is directly connected to a load R_{load}. Changes in load are simulated by modifying the variable resistance according to $R_{\text{load}} = V_{\text{fc}}^2/P_{\text{load,ref}}$. The SOFC initially is in steady state supplying a load of 3 kW. At time instant 20 s, the reference load profile $P_{\text{load,ref}}$ increases to 5 kW at a rate of 1000 W/s. At 60 s, $P_{\text{load,ref}}$ decreases at that rate to a final value of 3 kW, as shown in the top plot of Fig. 13.

When the SOFC starts to generate electric power, the SOFC exhaust stream is used to preheat the SOFC inlet air and hydrogen flows using the two preheaters, also contained in the block "SOFC based CHP". After the process of preheating, the SOFC exhaust stream still has valuable thermal energy. This remaining exhaust stream is delivered to the block "Heat exchanger power stage" using a pipe for warming up domestic water. The temperature of the stream $T^{\text{hex}}_{\text{i,exh}}$ is shown in the second plot of Fig. 13. The temperature is seen to change with the changes of the electric load. For instance, at time instant 20 s, the SOFC-CHP generates more electric power to meet the increase of the electric load. At the same time, a large thermal energy transfer is obtained from the CHP as well, leading to the increase of the temperature $T^{\text{hex}}_{\text{i,exh}}$ at the input of the heat exchanger power stage.

B. Thermal and Flow Transients of Domestic Water Supply

The third plot of Fig. 13 shows the transients of the domestic hot water temperature $T^{\text{hex}}_{\text{o,dw}}$ after the heat exchanger. Due to the implemented control, this temperature is set to stay around 323 K for comfortable hot water usage [24]. The magnitude of the deviation remains less than 2 K. The description of the control is detailed in the Appendix B. The flow rate of the domestic water $\dot{m}_{\text{dw}}$ is adjusted by regulating the valve in the heat exchanger to maintain the temperature of the hot water supply. The transients of the domestic water flow rate are presented in the fourth plot of Fig. 13. In the heat exchanger, the heat transfer rate $\dot{Q}_{\text{dw}}$ from the exhaust stream to the domestic water is also given in Fig. 13. As expected, $\dot{Q}_{\text{dw}}$ rises with the exhaust stream temperature $T^{\text{hex}}_{\text{i,exh}}$. A higher $T^{\text{hex}}_{\text{i,exh}}$ leads to a larger enthalpy transfer $\dot{H}^{\text{hex}}_{\text{o,dw}}$.

VII. Conclusions

A new methodology for modeling the enthalpy transfer using electric circuit elements was developed, implemented, and applied to the simulation of multi-physics power systems involving multiple energy carriers. The presented work is distinguished through three contributions. First, the concept of the enthalpy transfer modeling using circuit equivalents was established. Second, it was shown how the implementation of the analogy can be applied in the modeling of the pipe for enthalpy transfer. Third, the performed validation shows the pipe model closely matching the real-world counterpart for steady state and for different transients. The implementation of the enthalpy transfer through electric circuit equivalents in an EMTP-type program enables the analysis of diverse transients in combined heat and power applications.

Appendix A
Assumptions

To facilitate the modeling of the CHP components, the following assumptions are made:

1) Junctions are nodes and do neither store mass nor energy.
2) In the control volumes of pipes and heat exchangers, conservation of mass applies; thus, the mass does not change inside the control volume.
3) In the control volumes of pipes and heat exchangers, changes in potential or kinetic energies are not considered.

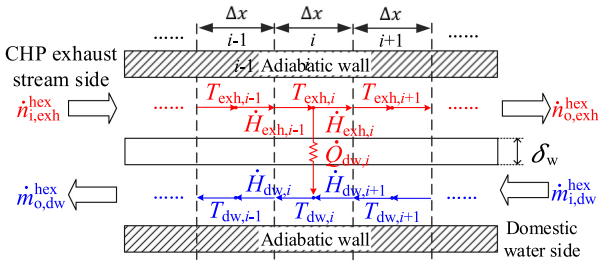

Fig. 14. Heat exchanger schematic showing flows and temperatures.

4) Pipes are circular and one-dimensional in the direction of the flow. Heat conduction between the fluids in the neighbouring control volumes of the pipe is neglected compared with energy transfer by advection.
5) The fluids are incompressible and of constant property.
6) Flows are considered in the fully developed region.
7) Radiation effects in heat exchanger are neglected compared with the heat transfer by convection and conduction.
8) In the storage tank used in the application, the temperature is uniformly distributed in the water.
9) The storage tank used in the application is lossless.

APPENDIX B
MODELING AND IMPLEMENTATION OF CHP COMPONENTS

Supplementary information on the modeling of the CHP application of Fig. 12 is given hereafter.

A. Heat Exchanger System

The heat exchanger system is composed of the block "Heat exchanger control stage" and the block "Heat exchanger power stage" of Fig. 12. The heat exchanger used in the application is a plate heat exchanger. A cross section of a heat exchanger representation after discretization [31] is shown in Fig. 14. The presented heat exchanger has one wall plate and is split into M segments. The CHP exhaust stream flows on the upper side of the heat exchanger, while the domestic water is warmed up on the lower side. Regarding the control volume i, the energy balances for both CHP exhaust stream and domestic water can be written as [31]:

$$\dot{Q}_{\mathrm{dw},i} = \dot{H}_{\mathrm{exh},i-1} - \dot{H}_{\mathrm{exh},i}, \tag{31}$$

$$\dot{Q}_{\mathrm{dw},i} = \dot{H}_{\mathrm{dw},i} - \dot{H}_{\mathrm{dw},i+1}, \tag{32}$$

where $\dot{Q}_{\mathrm{dw},i}$ is the heat transferred from the CHP exhaust stream to the flowing domestic water; $\dot{H}_{\mathrm{exh},i-1}$ and $\dot{H}_{\mathrm{exh},i}$ are the inlet and outlet enthalpy transfers of the CHP exhaust stream within the control volume i, respectively; $\dot{H}_{\mathrm{dw},i+1}$ and $\dot{H}_{\mathrm{dw},i}$ are the inlet and outlet enthalpy transfers of the flowing domestic water, respectively. These energy transfers as shown in Fig. 14 can be expressed by:

$$\dot{H}_{\mathrm{exh},i} = \dot{n}_{\mathrm{exh}} \overline{h}(T_{\mathrm{exh},i}), \tag{33}$$

$$\dot{H}_{\mathrm{exh},i-1} = \dot{n}_{\mathrm{exh}} \overline{h}(T_{\mathrm{exh},i-1}), \tag{34}$$

$$\dot{H}_{\mathrm{dw},i} = \dot{m}_{\mathrm{dw}} h(T_{\mathrm{dw},i}), \tag{35}$$

$$\dot{H}_{\mathrm{dw},i+1} = \dot{m}_{\mathrm{dw}} h(T_{\mathrm{dw},i+1}), \tag{36}$$

$$\dot{Q}_{\mathrm{dw},i} = \frac{1}{R_{\mathrm{th,hex},i}}(T_{\mathrm{exh},i} - T_{\mathrm{dw},i}), \tag{37}$$

and

$$\dot{n}_{\mathrm{exh}} = \dot{n}^{\mathrm{hex}}_{i,\mathrm{exh}} \tag{38}$$

$$\dot{m}_{\mathrm{dw}} = \dot{m}^{\mathrm{hex}}_{i,\mathrm{dw}} \tag{39}$$

where h and $\overline{h}$ are the specific enthalpy and molar enthalpy, respectively [5], $R_{\mathrm{th,hex},i}$ is the overall thermal resistance in the heat exchanger regarding control volume i as shown in Fig. 14. Similar to the overall thermal resistance in the pipe, the heat exchanger overall thermal resistance also comprises several components:

$$R_{\mathrm{th,hex},i} = R_{\mathrm{th,hex,exh},i} + R_{\mathrm{th,hex,w},i} + R_{\mathrm{th,hex,dw},i}, \tag{40}$$

where $R_{\mathrm{th,hex,exh},i}$ is the hot fluid side convection thermal resistance of the segment, $R_{\mathrm{th,hex,w},i}$ is the heat exchanger wall thermal resistance of the segment, and $R_{\mathrm{th,hex,dw},i}$ is the cold fluid side convection thermal resistance of the segment. They can be expressed as:

$$R_{\mathrm{th,hex,exh},i} = \frac{1}{k_{\mathrm{conv,exh},i} A_{\mathrm{exh},i}}, \tag{41}$$

$$R_{\mathrm{th,hex,w},i} = \frac{\delta_{\mathrm{w}}}{k_{\mathrm{cond,w},i} A_{\mathrm{w},i}}, \tag{42}$$

$$R_{\mathrm{th,hex,dw},i} = \frac{1}{k_{\mathrm{conv,dw},i} A_{\mathrm{dw},i}}, \tag{43}$$

where $A_{\mathrm{exh},i}$ and $A_{\mathrm{dw},i}$ are the surface areas of exhaust stream side and domestic water side, respectively, of a heat exchanger segment, $A_{\mathrm{w},i}$ is the wall area of a heat exchanger segment, and δ_{w} is the wall plate thickness.

The pressure drop in the flow direction in the heat exchanger segment due to wall friction can be calculated by:

$$\Delta p_{\mathrm{fl,exh},i} = R_{\mathrm{fl,exh},i} \dot{n}_{\mathrm{exh}}, \tag{44}$$

$$\Delta p_{\mathrm{fl,dw},i} = R_{\mathrm{fl,dw},i} \dot{m}_{\mathrm{dw}}, \tag{45}$$

and

$$R_{\mathrm{fl,exh},i} = K_{\mathrm{exh}} |\dot{n}_{\mathrm{exh}}|, \tag{46}$$

$$R_{\mathrm{fl,dw},i} = K_{\mathrm{dw}} |\dot{m}_{\mathrm{dw}}|, \tag{47}$$

where K_{exh} and K_{dw} are the pressure loss coefficients of exhaust stream side and domestic water side, respectively, in the heat exchanger.

For domestic hot water preparation, it is important to design a controller that maintains the temperature of the supplied water at a comfortable level. This is accomplished by using a proportional integral (PI) controller to regulate the inlet water flow to the heat exchanger. The input error signal ε to the PI controller is calculated as follows:

$$\varepsilon = (T^{\mathrm{hex}}_{\mathrm{o,dw}} - T_{\mathrm{dw,ref}}), \tag{48}$$

where $T_{\mathrm{dw,ref}}$ is the desired reference hot water temperature.

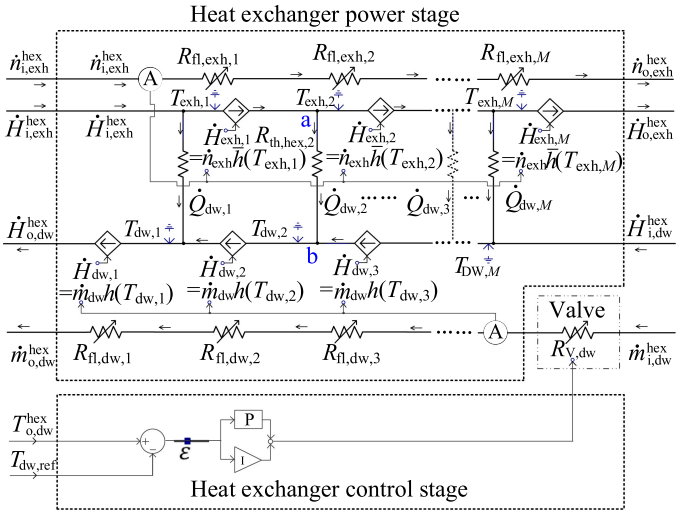

Fig. 15. Implementation of heat exchanger in PSCAD.

The implementation of the heat exchanger power stage using circuit equivalents is depicted in the upper part of Fig. 15. The implementation of control volume $i = 2$ with the two electrical nodes 'a' and 'b', as shown in the figure, is considered as an example for illustrative purposes. In accordance with Fig. 14, the CHP exhaust stream $\dot{n}_{\mathrm{i,exh}}^{\mathrm{exh}}$ enters from the left. Three energy transfers meet at node 'a' in order to satisfy (31). The enthalpy transfers $\dot{H}_{\mathrm{exh},1}$ and $\dot{H}_{\mathrm{exh},2}$ are modeled as two current-controlled current sources. The controlling signals are depicted in the figure according to (33) and (34). The heat transfer $\dot{Q}_{\mathrm{dw},2}$ from node 'a' to node 'b' passes through the thermal resistance $R_{\mathrm{th,hex},2}$. It represents the heat transferred from the exhaust stream to the flowing domestic water and is based on (37). Similarly, three energy transfers meet at node 'b' in order to model (32). One of these transfers is $\dot{Q}_{\mathrm{dw},2}$. The other two enthalpy transfers $\dot{H}_{\mathrm{dw},2}$ and $\dot{H}_{\mathrm{dw},3}$ are also modeled as current-controlled current sources, whose controlling signals are given in the figure based on (35) and (36). Regarding the mass flows of the fluids, the representations are depicted by the circuits in parallel. The pressure drop of the domestic water flowing in the heat exchanger segment is represented by the voltage drop across the flow resistance $R_{\mathrm{fl,dw},i}$. The pressure drop of the exhaust stream is given by the voltage drop across $R_{\mathrm{fl,exh},i}$.

The valve used for regulating the flow rate of the domestic water is modeled as a variable resistance. It is adjusted by the PI controller that is implemented in the lower part of Fig. 15.

B. Domestic Water Supply and Storage

Regarding the domestic water supply unit, a pressure source drives the domestic water inlet flow as depicted in Fig. 16. The flow rate of the domestic water is regulated by adjusting the valve of the heat exchanger as explained above. The enthalpy transfer of this water flow is calculated by:

$$\dot{H}_{\mathrm{dw}}^{\mathrm{src}} = \dot{m}_{\mathrm{dw}}^{\mathrm{src}} \cdot h(T_{\mathrm{dw}}^{\mathrm{src}}), \tag{49}$$

where 'src' stands for source.

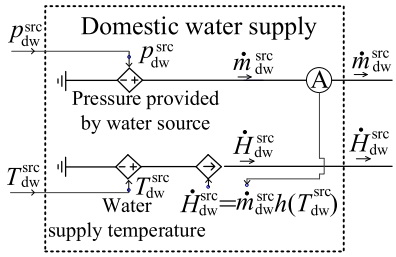

Fig. 16. Implementation of domestic water supply in PSCAD.

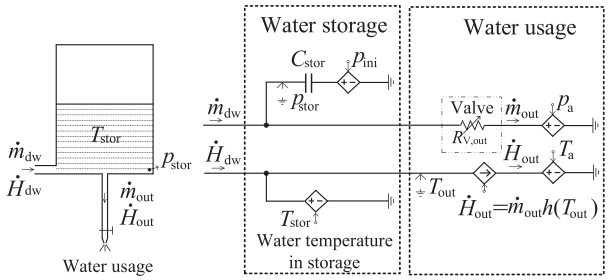

Fig. 17. Diagram and implementation of domestic water storage and usage in PSCAD.

The generated domestic hot water is stored in a tank for the future water usage. This storage is assumed to be a cylindrical isolated water tank as depicted in the left part of Fig. 17. The water pressure in the storage p_{stor} is given by [24], [32]:

$$\frac{\mathrm{d}p_{\mathrm{stor}}}{\mathrm{d}t} = \frac{1}{C_{\mathrm{stor}}}(\dot{m}_{\mathrm{dw}} - \dot{m}_{\mathrm{out}}), \tag{50}$$

and

$$C_{\mathrm{stor}} = \frac{\pi r_{\mathrm{stor}}^2}{\mathrm{g}}, \tag{51}$$

where C_{stor} is the hydraulic capacitance [3], r_{stor} is the radius of the storage tank, g is the gravitational acceleration. In the time interval of the simulation in Section VI, the future water usage is not considered, leading to $\dot{m}_{\mathrm{out}} = 0$.

As depicted in the left part of Fig. 17, T_{stor} is the temperature of the water in the tank according to assumption 8 of Appendix A. Then, the total enthalpy H_{stor} of the water stored in the tank can be expressed by [5]:

$$H_{\mathrm{stor}} = m_{\mathrm{stor}} h(T_{\mathrm{stor}}), \tag{52}$$

and m_{stor} is the total mass of the water stored in the tank:

$$m_{\mathrm{stor}} = \int_{t_{\mathrm{ini}}}^{t} \dot{m}_{\mathrm{dw}} \mathrm{d}\tau + m_{\mathrm{ini}}, \tag{53}$$

where $\dot{m}_{\mathrm{dw}}$ is the mass flow of domestic hot water feeding the tank, and m_{ini} is the initial mass of the water stored in the tank at time instant t_{ini}. If the tank is empty at the beginning of the simulation, then $m_{\mathrm{ini}} = 0$.

According to assumption 9 of Appendix A, enthalpy H_{stor} can be calculated by:

$$H_{\mathrm{stor}} = \int_{t_{\mathrm{ini}}}^{t} \dot{H}_{\mathrm{dw}} \mathrm{d}\tau + m_{\mathrm{ini}} h(T_{\mathrm{ini}}), \tag{54}$$

where $\dot{H}_{\mathrm{dw}}$ is the enthalpy transfer affiliated with $\dot{m}_{\mathrm{dw}}$, T_{ini} is the temperature of the water in the storage at the beginning of the simulation. Combining (52), (53), and (54), the average temperature of the water T_{stor} in the tank can be obtained.

The implementation of the water storage is depicted in the right part of Fig. 17. In the lower part, the controllable voltage source with controlling signal of T_{stor} is used for indicating the temperature of the water in the tank. In the upper circuit, the hydraulic circuit is implemented according to (50). The controllable voltage source with controlling signal p_{ini} is used for indicating the initial water pressure in the tank. This pressure can be calculated as: $p_{\mathrm{ini}} = \rho g z_{\mathrm{ini}}$. Here, z_{ini} is the initial depth of the water in the tank.

REFERENCES

[1] A. V. Luikov, *Analytical Heat Diffusion Theory*, New York, NY, USA: Academic, 2012.

[2] D. C. Karnopp, D. L. Margolis, and R. C. Rosenberg, *System Dynamics: Modeling, Simulation, and Control of Mechatronic Systems*, New York, NY, USA: Wiley, 2012.

[3] R. H. Bishop, *Mechatronic systems, Sensors, and Actuators: Fundamentals and Modeling*, New York, NY, USA: CRC Press, 2007.

[4] Y. A. Cengel, *Introduction to Thermodynamics and Heat Transfer*, New York, NY, USA: McGraw-Hill, 1997.

[5] M. J. Moran, H. N. Shapiro, D. D. Boettner, and M. B. Bailey, *Fundamentals of Engineering Thermodynamics*, New York, NY, USA: Wiley, 2010.

[6] U. S. Department of Energy, "Combined Heat and Power (CHP) Technical Potential in the United States," Washington, DC, USA, Rep. DOE/EE-1328, Mar. 2016.

[7] G. Angrisani, C. Roselli, and M. Sasso, "Distributed microtrigeneration systems," *Prog. Energ. Combust.*, vol. 38, no. 4, pp. 502–521, 2012.

[8] P. Mancarella, "MES (multi-energy systems): An overview of concepts and evaluation models," *Energy*, vol. 65, pp. 1–17, Feb. 2014.

[9] F. Zhao, C. Zhang, and B. Sun, "Initiative optimization operation strategy and multi-objective energy management method for combined cooling heating and power," *IEEE/CAA J. Autom. Sinica*, vol. 3, no. 4, pp. 385–393, Oct. 2016.

[10] S. Clegg and P. Mancarella, "Integrated electrical and gas network flexibility assessment in low-carbon multi-energy systems," *IEEE Trans. Sustain. Energy*, vol. 7, no. 2, pp. 718–731, Apr. 2016.

[11] X. Liu, J. Wu, N. Jenkins, and A. Bagdanavicius, "Combined analysis of electricity and heat networks," *Applied Energy*, vol. 162, pp. 1238–1250, 2016.

[12] S. Pazouki, A. Mohsenzadeh, S. Ardalan, and M. R. Haghifam, "Optimal place, size, and operation of combined heat and power in multi carrier energy networks considering network reliability, power loss, and voltage profile," *IET Gener. Transmiss. Distrib.*, vol. 10, no. 7, pp. 1615–1621, Dec. 2016.

[13] H. W. Dommel, "Digital computer solution of electromagnetic transients in single- and multiphase networks," *IEEE Trans. Power App. Syst.*, vol. PAS-88, no. 4, pp. 388–399, Apr. 1969.

[14] A. M. Gole, O. B. Nayak, T. S. Sidhu, and M. S. Sachdev, "A graphical electromagnetic simulation laboratory for power systems engineering programs," *IEEE Trans. Power Syst.*, vol. 11, no. 2, pp. 599–606, May 1996.

[15] K. Strunz and E. Carlson, "Nested fast and simultaneous solution for time-domain simulation of integrative power-electric and electronic systems," *IEEE Trans. Power Del.*, vol. 22, no. 1, pp. 277–287, Jan. 2007.

[16] S. Filizadeh, M. Heidari, A. Mehrizi-Sani, J. Jatskevich, and J. Martinez, "Techniques for interfacing electromagnetic transient simulation programs with general mathematical tools IEEE taskforce on interfacing techniques for simulation tools," *IEEE Trans. Power Del.*, vol. 23, no. 4, pp. 2610–2622, Oct. 2008.

[17] C. Wang, M. H. Nehrir, and S. R. Shaw, "Dynamic models and model validation for PEM fuel cells using electrical circuits," *IEEE Trans. Energy Convers.*, vol. 20, no. 2, pp. 442–451, Jun. 2005.

[18] W. H. Tang, Q. H. Wu, and Z. J. Richardson, "A simplified transformer thermal model based on thermal-electric analogy," *IEEE Trans. Power Del.*, vol. 19, no. 3, pp. 1112–1119, Jul. 2004.

[19] S. A. Ryder and I. J. Vaughan, "A simple method for calculating core temperature rise in power transformers," *IEEE Trans. Power Del.*, vol. 19, no. 2, pp. 637–642, Apr. 2004.

[20] G. Swift, T. S. Molinski, and W. Lehn, "A fundamental approach to transformer thermal modeling—Part I: Theory and equivalent circuit," *IEEE Trans. Power Del.*, vol. 16, no. 2, pp. 171–175, Apr. 2001.

[21] D. Susa and M. Lehtonen, "Dynamic thermal modeling of power transformers: Further development – Part I," *IEEE Trans. Power Del.*, vol. 21, no. 4, pp. 1961–1970, Oct. 2006.

[22] R. Isermann, *Mechatronic Systems: Fundamentals*, London, U.K.: Springer-Verlag, 2005.

[23] B. A. Finlayson, *Numerical Methods for Problems With Moving Fronts*. Seattle, WA, USA: Ravenna Park Publishing, 1992.

[24] S. Frederiksen and S. Werner, *District Heating and Cooling*, 1st ed. Lund, Sweden: Studentlitteratur AB, 2013.

[25] K. Strunz, E. Abbasi, and D. N. Huu, "DC microgrid for wind and solar power integration," *IEEE J. Emerg. Sel. Top. Power Electron.*, vol. 2, no. 1, pp. 115–126, Mar. 2014.

[26] A. Yazdani *et al.*"Modeling guidelines and a benchmark for power system simulation studies of three-phase single-stage photovoltaic systems," *IEEE Trans. Power Del.*, vol. 26, no. 2, pp. 1247–1264, Apr. 2011.

[27] V. D. Stevanovic, B. Zivkovic, S. Prica, B. Maslovaric, V. Karamarkovic, and V. Trkulja, "Prediction of thermal transients in district heating systems," *Energy Convers. Manage.*, vol. 50, no. 9, pp. 2167–2173, Sep. 2009.

[28] T. Lan and K. Strunz, "Multi-physics transients modeling of solid oxide fuel cells: Methodology of circuit equivalents and use in EMTP-type power system simulation," *IEEE Trans. Energy Convers.*, vol. 32, no. 4, pp. 1309–1321, Dec. 2017.

[29] C. Wang and M. H. Nehrir, "A physically based dynamic model for solid oxide fuel cells," *IEEE Trans. Energy Convers.*, vol. 22, no. 4, pp. 887–897, Dec. 2007.

[30] R. Ma, F. Gao, E. Breaz, Y. Huangfu, and P. Briois, "Multi-dimensional reversible solid oxide fuel cell modeling for embedded applications," *IEEE Trans. Energy Convers.*, vol. 33, no. 2, pp. 692–701, Jun. 2018.

[31] R. K. Shah and D. P. Sekulic, *Fundamentals of Heat Exchanger Design*, New York, NY, USA: Wiley, 2003.

[32] C. M. Colson and M. H. Nehrir, "Evaluating the benefits of a hybrid solid oxide fuel cell combined heat and power plant for energy sustainability and emissions avoidance," *IEEE Trans. Energy Convers.*, vol. 26, no. 1, pp. 140–148, Mar. 2011.

Tian Lan received master's degree in control theory and control engineering from TongJi University, Shanghai, China, in 2011, and the Dr.-Ing. degree (summa cum laude) from Technische Universität (TU) Berlin, Berlin, Germany, in 2016. He is currently working with Global Energy Interconnection Research Institute (GEIRI) Europe GmbH, Berlin, which is a subsidiary of State Grid Corporation of China (SGCC). His current research interests include fuel cells based combined heat and power system, multi-energy system, and eMobility.

Kai Strunz received the Dipl.-Ing. and Dr.-Ing. (summa cum laude) degrees from the Saarland University, Saarbrücken, Germany, in 1996 and 2001, respectively. From 1995 to 1997, he pursued research at Brunel University London, London, U.K. From 1997 to 2002, he worked at the Division Recherche et Développement of Electricité de France in Paris. From 2002 to 2007, he was an Assistant Professor of electrical engineering with the University of Washington in Seattle, WA, USA. Since September 2007, he is working as a Professor with the Institute of Sustainable Electric Networks and Sources of Energy, Technische Universität Berlin, Berlin, Germany.

Dr. Strunz is Guest Professor of the Institute of Electrical Engineering, Chinese Academy of Sciences. He is the Chairman of the IEEE Power and Energy Society (PES) Subcommittee on Distributed Energy Resources and the Chairman of the Subcommittee on Research in Education. He was the recipient of the IEEE PES Prize Paper Award in 2015 and the IEEE JOURNAL OF EMERGING AND SELECTED TOPICS IN POWER ELECTRONICS First Prize Paper Award in 2015.